Inorganic Chemistry
Article
pubs.acs.org/IC

Ligand-Bridged Dinuclear Cyclometalated Ir^{III} Complexes: From Metallamacrocycles to Discrete Dimers$^{\perp}$

Vadapalli Chandrasekhar,*[†] Tanima Hajra,[†] Jitendra K. Bera,*[†] S.M. Wahidur Rahaman,[†] Nisa Satumtira,[‡] Oussama Elbjeirami,[§] and Mohammad A. Omary*[‡]

[†]Department of Chemistry, Indian Institute of Technology Kanpur, Kanpur 208016, India
[‡]Department of Chemistry, University of North Texas, Box 305070, Denton, Texas 76203-5070, United States
[§]Department of Chemistry, King Fahd University of Petroleum & Minerals, Dhahran, 31261 Kingdom of Saudi Arabia

S Supporting Information

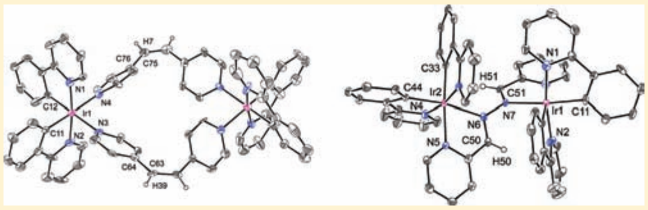

ABSTRACT: Metallamacrocycles **1**, **2**, and **3** of the general formula $[\{\mathrm{Ir}(ppy)_2\}_2(\mu\text{-BL})_2](\mathrm{OTf})_2$ (*ppy*H = 2-phenyl pyridine; BL = 1,2-bis(4-pyridyl)ethane (*bpa*) (**1**), 1,3-bis(4-pyridyl)propane (*bpp*) (**2**), and *trans*-1,2-bis(4-pyridyl)-ethylene (*bpe*) (**3**)) have been synthesized by the reaction of $[\{(\mathrm{ppy})_2\mathrm{Ir}\}_2(\mu\text{-Cl})_2]$, first with AgOTf to effect dechlorination and later with various bridging ligands. Open-frame dimers $[\{\mathrm{Ir}(\mathrm{ppy})_2\}_2(\mu\text{-BL})](\mathrm{OTf})_2$ were obtained in a similar manner by utilizing *N,N′*-bis(2-pyridyl)methylene-hydrazine (*abp*) and *N,N′*-(bis(2-pyridyl)formylidene)ethane-1,2-diamine (*bpfd*) (for compounds **4** and **5**, respectively) as bridging ligands. Molecular structures of **1**, **3**, **4**, and **5** were established by X-ray crystallography. Cyclic voltammetry experiments reveal weakly interacting "$\mathrm{Ir}(\mathrm{ppy})_2$" units bridged by ethylene-linked *bpe* ligand in **3**; on the contrary the metal centers are electronically isolated in **1** and **2** where the bridging ligands are based on ethane and propane linkers. The dimer **4** exhibits two accessible reversible reduction couples separated by 570 mV indicating the stability of the one-electron reduced species located on the diimine-based bridge *abp*. The "$\mathrm{Ir}(\mathrm{ppy})_2$" units in compound **5** are noninteracting as the electronic conduit is truncated by the ethane spacer in the *bpfd* bridge. The dinuclear compounds **1**−**5** show ligand centered (LC) transitions involving *ppy* ligands and mixed metal to ligand/ligand to ligand charge transfer (MLCT/LLCT) transitions involving both the cyclometalating *ppy* and bridging ligands (BL) in the UV−vis spectra. For the conjugated bridge *bpe* in compound **3** and *abp* in compound **4**, the lowest-energy charge-transfer absorptions are red-shifted with enhanced intensity. In accordance with their similar electronic structures, compounds **1** and **2** exhibit identical emissions. The presence of vibronic structures in these compounds indicates a predominantly ^{3}LC excited states. On the contrary, broad and unstructured phosphorescence bands in compounds **3**−**5** strongly suggest emissive states of mixed ^{3}MLCT/^{3}LLCT character. Density functional theory (DFT) calculations have been carried out to gain insight on the frontier orbitals, and to rationalize the electrochemical and photophysical properties of the compounds based on their electronic structures.

■ INTRODUCTION

Ligand-bridged bimetallic complexes containing second and third row transition metal ions have attracted considerable interest because of their exquisite electronic and electrochemical properties.[1]

Although several reports of dinuclear Ru(II), Pd(II), Pt(II), and Os(II) compounds are known in the literature,[2] limited studies are reported on Ir(III) systems.[3] It occurred to us that "$\mathrm{Ir}(ppy)_2$" (*ppyH* = 2-phenyl pyridine) motifs containing two vacant coordination sites would serve as excellent building blocks for the construction of bimetallic Ir(III) compounds including the possibility of realizing Ir^{III}-containing macrometallacycles. Further, "$\mathrm{Ir}(ppy)_2$" motifs exhibit rich photophysical properties,[4] and it was anticipated that the resulting bimetallic derivatives might possess interesting optical properties. The demonstrated ability of the pyridine-based linkers for the construction of dinuclear structures prompted us to employ the set of ligands, as shown in Scheme 1, in this work. The choice of bridging ligands was based on the following

Scheme 1. Bis-pyridyl Linkers Employed in This Work

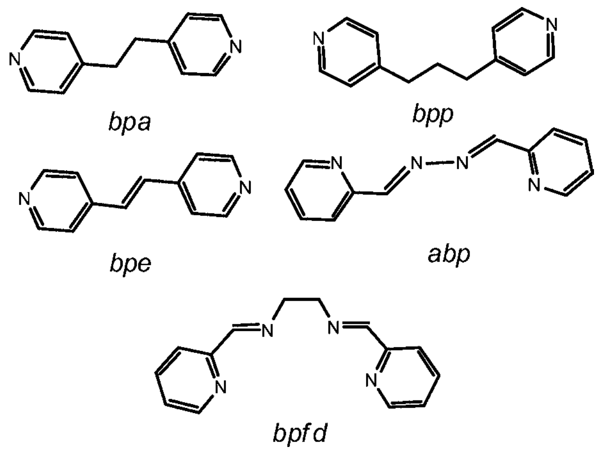

Received: June 16, 2011
Published: January 18, 2012

considerations: (1) variation of the spacer length between the pyridyl donor atoms would modulate the intermetallic distances, and (2) the extent of the bridging ligand conjugation would dictate the degree of metal—metal interaction. The most attractive feature of the diiridium complexes that could be fashioned from this approach is the possibility of color tuning and modulating the lifetime of emissions by variation of the ligand (conjugated vs nonconjugated, chelating vs nonchelating). Accordingly, herein, we describe the synthesis, structural characterization, electrochemical and photophysical studies of various diiridium complexes containing "Ir(*ppy*)$_2$" units that are bridged by bis-pyridyl linkers. The use of bridging ligands, 1,2-bis(4-pyridyl)-ethane (*bpa*), 1,3-bis(4-pyridyl)propane (*bpp*), and *trans*-1,2-bis(4-pyridyl)ethylene (*bpe*) afforded metallamacrocycles consisting of two noninteracting "Ir(ppy)$_2$" units, while using *N*,*N*′-bis(2-pyridyl)methylene-hydrazine (*abp*) and *N*,*N*′-(bis(2-pyridyl)formylidene)ethane-1,2-diamine (*bpfd*) results in discrete dimers. Density functional theory (DFT) calculations were undertaken to gain insight into the electronic structures of these compounds and also to rationalize their photophysical behavior.

RESULTS AND DISCUSSION

Synthetic Aspects. The cyclometalated Ir(III) dimer $[\{(ppy)_2\text{Ir}\}_2(\mu\text{-Cl})_2]$ was chosen as the precursor for further elaboration.[5] The reaction of this chloro-bridged dimer first with AgOTf, to effect dechlorination, followed by treatment with the bridging ligands, afforded ligand-bridged derivatives $[\{\text{Ir}(ppy)_2\}_2(\mu\text{-}bpa)_2](\text{OTf})_2$ (**1**), $[\{\text{Ir}(ppy)_2\}_2(\mu\text{-bpp})_2](\text{OTf})_2$ (**2**), $[\{\text{Ir}(ppy)_2\}_2(\mu\text{-}bpe)_2](\text{OTf})_2$ (**3**), $[\{\text{Ir}(ppy)_2\}_2(\mu\text{-}abp)](\text{OTf})_2$ (**4**), and $[\{\text{Ir}(ppy)_2\}_2(\mu\text{-}bpfd)](\text{OTf})_2$ (**5**) in very good yields (see Experimental Section). Unlike other compounds, metallacycle **3** could be obtained in a pure form only after repeated crystallizations. Molecular structures of **1**, **3**, **4**, and **5** have been unambiguously determined by single crystal X-ray diffraction studies. Appropriate single crystals of **2** could not be obtained; however, it could be characterized by analytical and spectroscopic techniques. Further, a DFT optimized structure of **2** was computed.

Compounds **1**−**5** contain bimetallic dicationic cores with triflate counteranions; the latter exhibit characteristic strong stretching vibrations in the region of 1260−1270 cm^{-1}.[6] ^{1}H NMR spectra of **1**−**5** exhibit complex multiplet patterns. Unambiguous assignment of the NMR signals could not be carried out because of extensive overlap of peaks. This complexity in the ^{1}H NMR spectra arises because of the presence of three possible isomers, one meso (Δ, Λ) and two enantiomeric pairs (Λ, Λ and Δ, Δ).[7]

Solid State Structures. The molecular structures of **1**, **3**, **4**, and **5** have been determined by X-ray crystallography. Details of data collection and refinement procedures are discussed in the Experimental Section. Relevant bond distances and angles are compared in Table 1.

The molecular structure of **1** consists of two organometallic "Ir(*ppy*)$_2$" subunits that are bridged by two *bpa* linkers. This results in the formation of a 22-membered metallamacrocycle (Figure 1). Only half of the molecule is observed in the asymmetric unit which is related to the other half by a crystallographically imposed C_2 symmetry. Each iridium center exhibits a slightly distorted octahedral geometry. Four of the

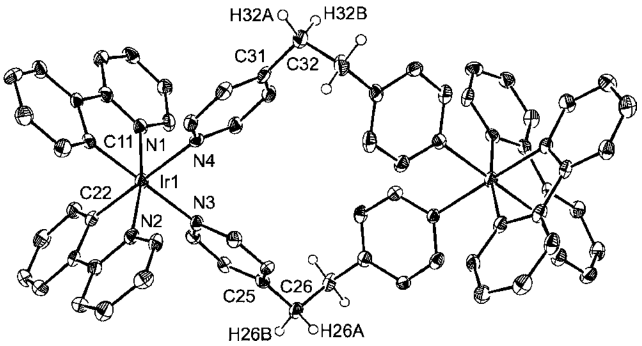

Figure 1. ORTEP diagram (40% probability thermal ellipsoids) of the dicationic unit $[\{\text{Ir}(ppy)_2\}_2(\mu\text{-}bpa)_2]$ in **1** with important atoms labeled. Hydrogen atoms are omitted for the sake of clarity (except the ethane hydrogens).

Table 1. Comparison of Relevant Metrical Parameters for Compounds 1, 3−5

	1		3		4		5	
Ir···Ir	9.878(1)		10.007(1)		5.124(1)		6.996(1)	
Ir(*ppy*)$_2$	Ir1−N1	Ir1−N2	Ir1−N1	Ir1−N2	Ir1−N1	Ir1−N2	Ir1−N1	Ir1−N2
	2.059(4)	2.056(4)	2.001(15)	2.029(18)	2.052(5)	2.039(6)	2.045(4)	2.057(4)
	Ir1−C11	Ir1−C22	Ir1−C11	Ir1−C12	Ir1−C11	Ir1−C22	Ir1−C11	Ir1−C22
	2.007(5)	2.012(5)	2.02(2)	2.03(2)	2.009(6)	2.001(6)	2.008(5)	2.012(5)
Ir-bridge-Ir	Ir1−N3	Ir1−N4	Ir1−N3	Ir1−N4	Ir2−N5	Ir1−N7	Ir1−N3	Ir1−N4
	2.176(4)	2.167(4)	2.191(16)	2.154(16)	2.148(5)	2.149(5)	2.132(4)	2.140(4)
					Ir2−N6	Ir1−N8		
					2.166(5)	2.148(5)		
bridge	C26−C26	C32−C32	C62−C63	C74−C75	N6−N7.	N7−C51	N4−C28	N4−C29
	1.543(11)	1.533(10)	1.36(3)	1.36(3)	1.426(7)	1.279(8)	1.274(6)	1.448(6)
			Ir2−N5	Ir2−N8	N6−C50		C29−C29	C27−C28
			2.197(18)	2.170(16)	1.294(8)		1.529(9)	1.456(7)
	φ C25−C26−C26−C25		φ C71−C74−C75−C76		φ Ir1−N7−N6−Ir2		φ C27−C28−N4−C29	
	74.0(8)		5.0(4)		126.6(4)		178.8(4)	
	φ C31−C32−C32−C31		φ C64−C63−C62−C59		φ C50−N6−N7−C51		φ N4−C29−C29−N4	
	71.3(9)		7.0(3)		126.2(6)		180.0	

six coordinating sites are occupied by two cyclometallating ppy ($C^{\wedge}N$) ligands. The remaining two sites contain the pyridyl nitrogen atoms from two independent linkers. The *cis*-C,C and *trans-N, N* chelate disposition of the *ppy* ligands of the chloro-bridged precursor complex is retained in **1**.[8] The pyridyl *N* atoms of the *bpa* linkers are trans to the metalated *C* atoms of ppy causing longer Ir−N(*bpa*) distances (2.176(4), 2.167(4) Å) than the corresponding Ir−N(ppy) distances (2.059(4), 2.056(4) Å). The intermolecular Ir···Ir distance is 9.878(1) Å.

The core structure of **3** is identical to **1** except that the "$Ir(ppy)_2$" subunits are bridged by the *shorter bpe* linker (Figure 2).

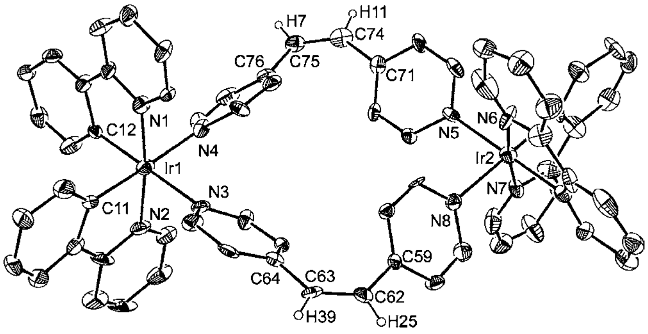

Figure 2. ORTEP diagram (40% probability thermal ellipsoids) of the dicationic unit $[\{Ir(ppy)_2\}_2(\mu\text{-}bpe)_2]$ in **3** with important atoms labeled. Hydrogen atoms are omitted for the sake of clarity (except the ethylene hydrogens).

In contrast to **1**, the asymmetric unit of **3** contains the full macrocycle. The coordination environment around Ir centers, the disposition of the *ppy* ligands, and the spanning of the *bpe* molecular bridge are very similar to that observed in **1**. In general, the trans isomers are the major species for an olefinic ligand such as *bpe* in its free form. Upon complexation, the *bpe* ligand adopts a cis geometry affording discrete metallacycles. The trans arrangement of the same ligand would have provided a polymeric structure which is entropically less favorable. The bond parameters observed in **1** and **3** are similar (Table 1). Contrary to our expectation, the shorter C−C bond distance of the ethylene spacer (1.36(3) Å) in the *bpe* linker results in a longer Ir···Ir separation (10.007(1) Å) in **3** than in **1** (9.878(1) Å). In the latter compound, the C−C distances of the ethane spacer are 1.533(10) and 1.543(11) Å.

Both **1** and **3**, as discussed above, are dinuclear metallamacrocycles. In each case, two $Ir(ppy)_2$ centers are connected to each other by the coordination action of two ditopic bridging ligands. In contrast, the molecular structure of **4** contains two organometallic "$(ppy)_2Ir$" subunits that are linked by a single *abp* bridge. This is made possible because the *abp* ligand contains two pockets of chelating coordinating environments on either end of the ligand. The coordination geometry around each Ir center is distorted octahedral. In addition to two *ppy* cyclometalating ligands, each Ir atom is coordinated to the *abp* ligand through a pyridyl *N* and an imine *N* resulting in a five-membered (IrN_2C_2) ring (Figure 3). Thus, each iridium atom is surrounded by a 2C, 4N coordination environment contained in three chelating rings. The *abp* bridge deviates considerably from planarity as reflected in the torsional angles C50−N6−N7−C51 (126.2(6)°) and Ir1−N7−N6−Ir2 (126.6(4)°). The imine C−N distances (1.294(8), 1.279(8) Å) and N6−N7 distance 1.426(7) Å are similar to those found in other metal-*abp* compounds.[9] The Ir···Ir separation of 5.124(1) Å is the shortest among other ligand-bridged "$Ir(ppy)_2$" dimers reported in this work in agreement with the fact that in this compound the two interconnected iridium centers are separated by only two intervening atoms.

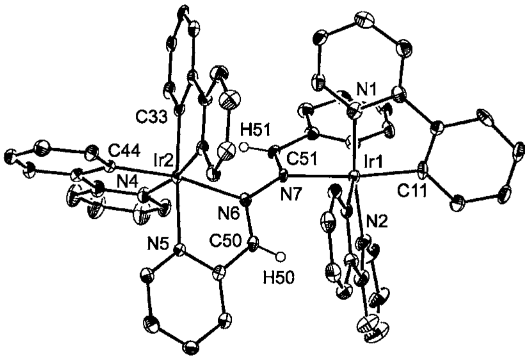

Figure 3. ORTEP diagram (40% probability thermal ellipsoids) of the dicationic unit $[\{Ir(ppy)_2\}_2(\mu\text{-}abp)]$ in **4** with important atoms labeled. Hydrogen atoms are omitted for the sake of clarity except the azine hydrogens.

The *bpfd* bridge in compound **5** contains an additional $-CH_2-CH_2-$ spacer that separates the two coordinating pockets of the ligand (Figure 4). The core structure of **5** is similar to **4** and consists of two organometallic "$(ppy)_2Ir$" subunits that are bridged by a *bpfd* linker. The asymmetric unit of **5** contains one-half of the dimeric unit which is related to the other half by a center of inversion. Each iridium center is part of three ring systems; two of these are formed as a result of coordination by the chelating *ppy* ligands. The third is formed by the coordination of the pyridyl and imine *N* donors of the *bpfd* ligand. Thus, each iridium is in a 2C, 4N coordination environment. The imine C−N distance (N4−C28 = 1.274(6) Å) in **5** is shorter than the corresponding distances observed in **4** (1.294(8), 1.279(8) Å). This observation is suggestive of the possibility of electron delocalization in the *abp* bridge in **4** which appears to be absent in the *bpfd* bridge in **5**. The consequence of the intervening $-CH_2-CH_2-$ spacer is also reflected in the longer Ir···Ir separation of 6.996(1) Å. A notable observation is that the bridging *bpfd* ligand is in a perfect *anti-* configuration as reflected in the crystallographically imposed torsional angle N4−C29−C29′−N4′ of 180°.

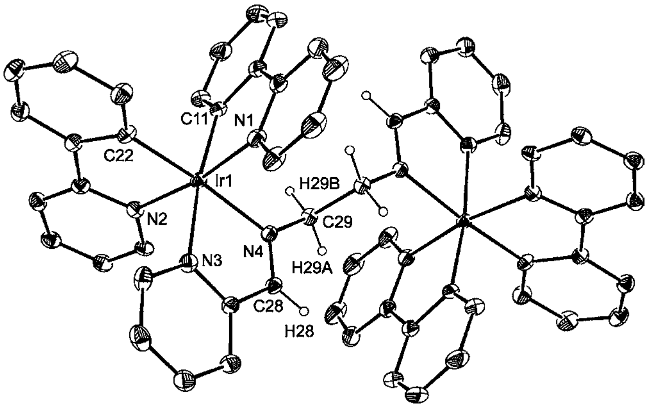

Figure 4. ORTEP diagram (40% probability thermal ellipsoids) of the dicationic unit $[\{Ir(ppy)_2\}_2(\mu\text{-}bpfd)]$ in **5** with important atoms labeled. Hydrogen atoms are omitted for the sake of clarity (except the azine and ethane hydrogens).

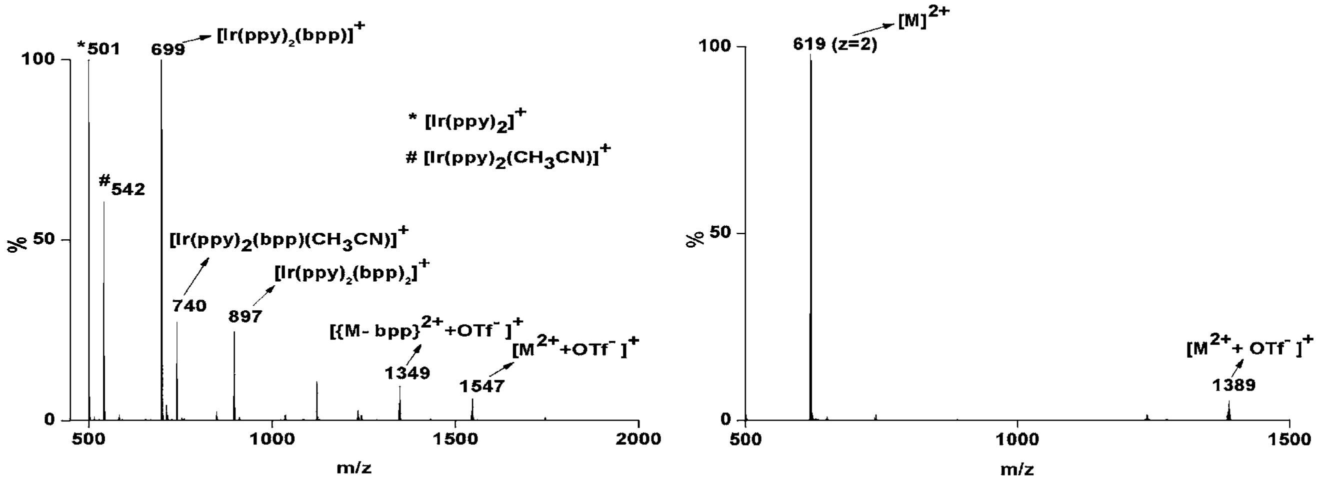

(a) (b)

Figure 5. ESI mass spectra for compounds (a) **2** and (b) **5**.

Mass Spectra. ESI mass spectral studies revealed that the dinuclear structures of compounds **1**−**5** are intact in solution. All compounds exhibit signals corresponding to the species $[\{M\}^{2+}+OTf^-]^+$, where $\{M\}^{2+}$ is the dicationic unit, although their relative intensities are less than 20%. As the molecular structure of **2** could not be established by X-ray crystallographic study, we examined its ESI-MS data more carefully. Complex **2** exhibits a signal at *m*/*z* 1547 (Figure 5a) which is assigned to $[\{M\}^{2+}+OTf^-]^+$ where (M = $[\{Ir(ppy)_2\}_2(bpp)_2]$). In addition, signals appear at *m*/*z* 1349, 897, and 740 which correspond to $[\{Ir_2(ppy)_4(bpp)\}^{2+}+OTf^-]^+$, $[Ir(ppy)_2(bpp)_2]^+$ and $[\{Ir(ppy)_2\}_2(bpp)(CH_3CN)]^+$. The highest intensity signals correspond to $[Ir(ppy)_2(bpp)]^+$ and $[Ir(ppy)_2]^+$ at *m*/*z* 699 and 501 respectively.

It is noteworthy to mention that the chelate-anchoring of the bridging ligands *abp* and *bpfd* in compounds **4** and **5** exhibit fewer signals, usually corresponding to molecular mass ions whereas the nonchelate bridging ligands (*bpa, bpp, and bpe*) in compounds **1**−**3** show fragmentation under identical experimental conditions. Comparison of electrospray ionization (ESI) mass spectra of the metallamacrocycle **2** and the dimer **5**, shown in Figure 5, attest to this differential behavior.

Electrochemistry. Electrochemical studies of compounds **1**−**5** were performed in acetonitrile and their redox potentials are summarized in Table 2. Compound **1** exhibits an irreversible metal-based oxidation at 1.43 V (Supporting Information, Figure S3). Two irreversible ligand based reductions are located at −1.03 and −1.61 V. The reduction event at the more negative potential is usually associated with the *ppy* ligands whereas the bridging *bpa* ligands are reduced at a less negative potential. This assignment is based on related iridium compounds.[10] The electrochemical behavior of compound **2** is identical to **1**. This is not surprising in view of the similarity of the bridging ligands present in these compounds.

Table 2. Electrochemical Data for Compounds 1−5 in Acetonitrile

compound	oxidation	reduction
1	1.43^a	−1.03^b, −1.61^b
2	1.43^a	−1.01^b, −1.60^b
3	1.07(180)^c, 1.38(140)^c	−0.51^b, −0.74^b, −1.19^b, −1.69^b
4	1.51^a, 1.70^a	−0.37(70)^c, −0.94(80)^c, −1.56^b
5	1.47^a	−1.07^b, −1.19^b, −1.63^b

^{a}Peak potentials, $E_{p,a}$, for irreversible processes. ^{b}Peak potentials, $E_{p,c}$, for irreversible processes. ^{c}Half-wave potentials evaluated from cyclic voltammetry as $E_{1/2} = (E_{p,a} + E_{p,c})/2$, peak potential differences in mV in parentheses.

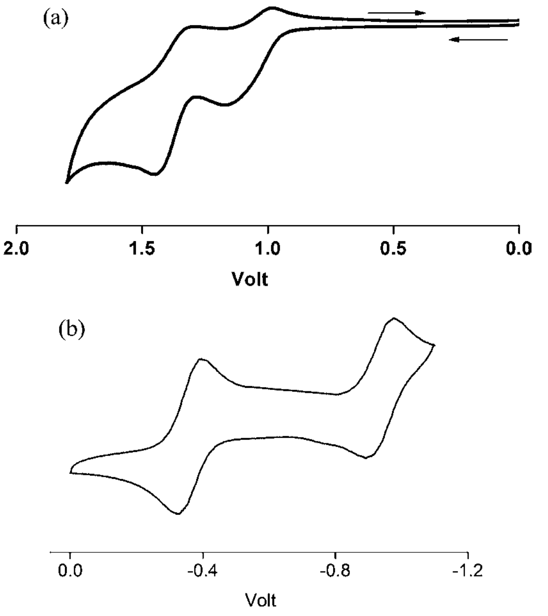

Figure 6. Cyclic voltammograms for (a) **3** and (b) **4** at a scan rate of 100 mV/s with 0.1 M $[Bu_4N][PF_6]$ as supporting electrolyte.

The presence of the ethylene spacer (−CH═CH−) in the *bpe* linker of **3** causes a significantly different response in its cyclic voltammetry. Two metal-based oxidation couples are observed at 1.07(180) and 1.38(140) V (Figure 6a). Large differences in the cathodic and anodic peak potentials and the corresponding currents indicate the quasi-reversible character of these events. Appearance of two oxidation waves suggests a weakly interacting dinuclear system through the *bpe* bridges. In addition, compound **3** exhibits multiple irreversible reductions. Reduction waves appearing in the range lower than −1.5 V are

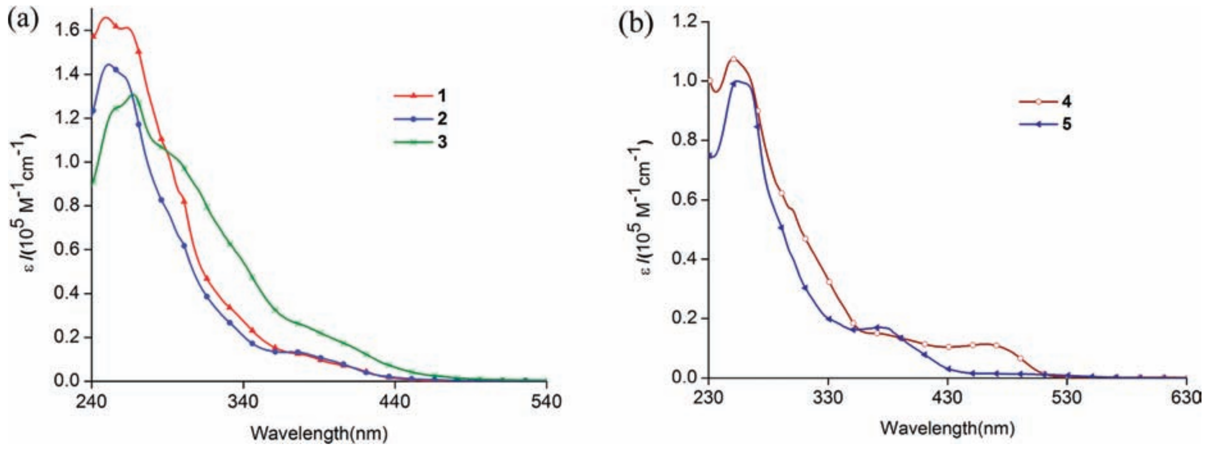

Figure 7. Absorption spectra of (a) **1**−**3** and (b) **4**, **5** in acetonitrile.

due to the *bpe* bridges while reduction at a more negative potential is associated with the cyclometalating *ppy* units.

Compound **4**, which contains the diimine spacer (−CH=N−N=CH−) in the bridging *abp* ligand, exhibits two reversible reduction couples at −0.37(70) and −0.94(80) V (Figure 6b) centered on the bridging ligand. The comproportionation constant ($K_c = 6.7 \times 10^9$), calculated from the difference of the sequential reduction potentials (570 mV), reflects the stability of the one-electron reduced species. Clearly this is an electron delocalized system in contrast to noninteracting Ir(*ppy*)$_2$ units in compounds **1** and **2**, or in the weakly coupled **3**. This is in accordance with the shortest Ir···Ir distance (5.124(1) Å) among all compounds reported here. An additional irreversible reduction wave at −1.56 V is attributed to *ppy* ligands. Two metal-based irreversible oxidations are also observed at 1.51 and 1.70 V.

Compound **5** exhibits a single irreversible metal-centered oxidation at 1.47 V (Supporting Information, Figure S4) and two closely spaced reductions at −1.07 and −1.19 V attributed to the *bpfd* bridge. A reduction process at a potential exceeding −1.5 V is also observed which is attributed to *ppy* ligands. The methylene spacer in the *bpfd* bridge evidently does not allow electronic coupling between the metal centers.

Photophysical Properties. *Absorption Studies.* The UV−vis spectra of compounds **1**−**5** are compared in Figure 7, and absorption data are compiled in Table 3. The concentration of all compounds was maintained at 10^{-5} M in acetonitrile solvent. Compound **1** exhibits intense absorptions in the UV at 249, 264, and 299 nm which are assigned to spin-allowed ligand centered (^{1}LC) transitions involving *ppy* ligands. An additional transition occurs at 380 nm extending up to 450 nm. Analysis of the frontier orbitals indicates a mixed metal to ligand/ligand to ligand charge transfer (MLCT/LLCT) transition for the low-energy band (vide infra). The absorption spectrum of compound **2** is similar in nature (Figure 7a). Clearly, increase in chain length of the spacer from ethane (**1**) to propane (**2**) does not show any significant effect on the energy as well as the intensity of the charge transfer absorptions. Further, the absorption characteristics are similar to related mononuclear cyclometalated Ir(III) complexes[4] indicating minimal involvement of the bridging ligands in the excited states. For compound **3**, introduction of the ethylene spacer causes two overlapped charge transfer bands at 384 and 425 nm with spin−orbit-coupled enhanced intensity (Figure 7a). The appearance of the low-energy band at 425 nm is indicative of an excited state with contribution from the bridging *bpe* ligands. DFT calculations support this assertion.

Table 3. Photophysical Properties of Compounds 1−5

compd.	absorption λ_{max} (nm) ($\varepsilon/10^5$ M^{-1} cm^{-1})	$\lambda_{max}{}^{em}$ (nm)	τ_p (μs)	Φ_p
1	249 (1.66), 264 (1.61), 299sh (0.84), 380 (0.12)	480, 510, 548	1.4	0.45
2	250 (1.44), 262 (1.39), 300sh (0.64), 381 (0.12)	480, 510, 548	1.8	0.48
3	256 (1.25), 267 (1.31), 296sh (1.01), 384(0.24), 425 (0.11)	538	5.9	0.41
4	251 (1.07), 374 (0.15), 465 (0.11)	521	4.1	0.51
5	254 (0.99), 376 (0.17)	525 (625)[a]	5.4 (6.0)	0.12

[a] Value in parentheses is for the crystalline solid.

Compound **4** exhibits intense absorptions between 250 to 350 nm which are assigned to ligand-based π−π* transitions (Figure 7b). In addition, two weaker bands of mixed MLCT/LLCT character appear at 374 and 465 nm. The absorption spectrum of **5** is similar to **4** except that the lowest energy band is missing in the former compound. Clearly, π-delocalized bridge (*abp* for compound **4**) results in a low-energy absorption beyond 450 nm which is missing for non- or truncated π-conjugated systems (e.g., *bpfd* for compound **5**).

Emission Studies. The photoluminescence of cyclometalated iridium complexes is characterized by emission from either a predominantly ^{3}LC state, a predominantly ^{3}MLCT, or a mixed ^{3}LC-^{3}MLCT state.[4d] The presence of vibronic structures indicates that the emissive excited states have a predominantly ^{3}LC character whereas broad and unstructured emissions are the characteristics of ^{3}MLCT or mixed ^{3}MLCT/^{3}LLCT states. All compounds prepared in this study are luminescent at room temperature, and the emission data are provided in Table 3. Excitation wavelengths were selected on the basis of the corresponding absorption spectra. For the sake of convenience, all spectra are compared in Figure 8.

The emission spectra of **1** and **2** are similar in nature. Both show blue emission at 480 and 510 nm as well as a shoulder at 548 nm when irradiated at 410 nm. The emission lifetimes of both complexes are in the microsecond region (1.4 and 1.8 μs for compound **1** and **2**, respectively) consistent with the emission from a triplet excited state. The photoluminescence quantum yields are estimated to be 0.45 and 0.48 respectively. The emission properties are similar to the monomer congener

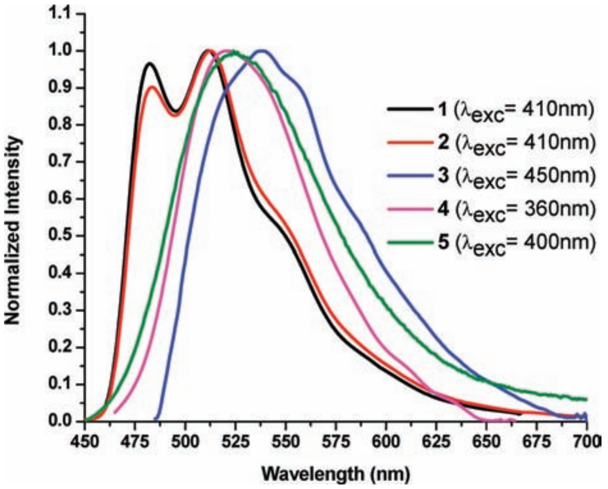

Figure 8. Emission spectra of **1**−**5** in acetonitrile. Excitation wavelengths are mentioned in parentheses.

$[\mathrm{Ir}(ppy)_2(py)_2]^+$.[11] The emissive state is likely to be ^{3}LC for **1** and **2** because of the clear vibronic structure.

Introduction of ethylene spacer in compound **3** causes a significant red-shifting of the emission spectrum. This compound shows a broad emission at 538 nm with a photoluminescence quantum yield 0.41. The corresponding emission lifetime is 5.9 μs. Broad and unstructured emission is indicative of an excited state with general charge transfer character in which the metal is involved (such as MLCT as the situation is well-known for Ru(II) polypyridyl complexes, or a metal-centered transition though it is unlikely for such d^6 complexes). Structured emission bands are more common with ligand-centered emissions. Although excited state calculations for the dinuclear complex could not be performed because of its large molecular size, DFT calculations on singlet ground state hint at an emissive state of mixed ^{3}MLCT/^{3}LLCT character. Further, Bernhard and co-workers have suggested mixed ^{3}MLCT and ^{3}LC excited state for a series of Ir(ppy)$_2$ complexes containing ancillary polypyridyl ligands.[12] The possibility of such an admixed emissive state for compound **3** cannot be ruled out. When both ligands contribute in the excited-state transitions, the cyclometalating ligand (ppy) tends to be associated with the ^{3}LC and the ancillary ligand (bpe) with the ^{3}MLCT states. Consistent with this mixed ^{3}MLCT/^{3}LC possible assignment for **3** is the fact that the emission profile is not very clearly resolved as the situation for **1** and **2** but cannot be described as completely unstructured as in **4** and **5**.

Compound **4** exhibits a featureless emission at 521 nm with a lifetime 4 μs. The degree of conjugation in the ancillary ligand is known to affect the lowest excited state. Accordingly, the emission is suggested to arise from a mixed ^{3}MLCT/^{3}LLCT state as opposed to ^{3}LC.

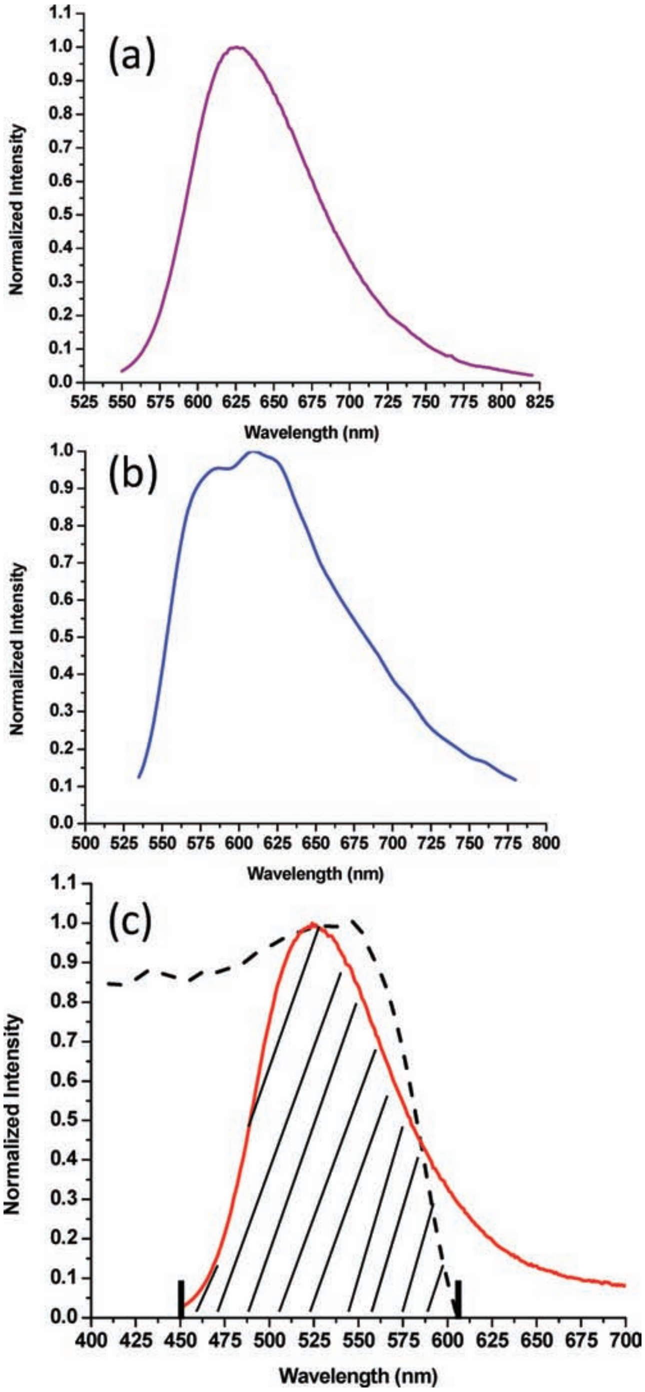

Figure 9. (a) Solid state photoluminescence spectrum of **5** (λ_{exc} = 465 nm) collected at 298 K. (b) Frozen solution (1: 3 acetonitrile: 2-methyl-tetrahydrofuran) photoluminescence spectrum of **5** (λ_{exc} = 490 nm) at 77 K. (c) Spectral overlap between the acetonitrile fluid solution emission spectrum (solid curve; λ_{exc} = 400 nm) and the solid-state photoluminescence excitation spectrum (dashed curve; λ_{em} = 670 nm) of **5** at 298 K.

Compound **5** exhibits fluid solution emission that is very similar in energy and unstructured profile to that of compound **4** so as to warrant a predominantly ^{3}MLCT assignment. Interestingly, however, the crystalline solid exhibits vastly red-shifted emission and excitation bands (Figure 9a) compared to the fluid solution bands. The solid was repeatedly crystallized from the same solutions ruling out impurities being the cause of this large energy difference. We tentatively attribute the different luminescence bands in fluid solution (Figure 8) versus the solid state (Figure 9a) to different structural conformers of **5**. The X-ray structure of **5** reveals an *anti-* crystallographic arrangement of the *bpfd* bridge. It is proposed that, in fluid solution, the C−C bond (C29−C29′) rotation leads to a new species in which the *bpfd* deviates from a strict *anti-* arrangement toward a *syn-* geometry. In a frozen rigid matrix, such a C−C rotation can be somewhat restricted giving rise to a significant population of the *anti-* conformer, which the lower cryogenic temperature can stabilize even if it were the less stable conformer. Indeed, measurements in frozen acetonitrile/2-methyl-tetrahydrofuran (1: 3) matrix at 77 K reveal a more similar emission profile to that for the solid instead of the fluid solution (Figure 9b). We notice that there is rather significant spectral overlap between the emission band of the fluid solution (assigned to the *syn*- conformer) and the excitation band of the solid material (assigned to the *anti*- conformer), as shown in Figure 9c. Therefore, when both conformers coexist, as is the situation we propose to be in a frozen matrix, energy transfer will lead to a greater dominance of the luminescence band for the *anti*- conformer, as seen experimentally for the frozen solution spectra (Figure 9b). We cannot completely rule out, however, solvation being a partial contributor to the difference between the luminescence behavior in solution versus the solid state of **5**. However, we notice only minor difference existed between the electronic spectra in coordinating versus non-coordinating solvents that are more likely explainable by the solvent polarity effects on charge transfer bands.

Computational Study. The dicationic units of compounds **1**−**5** were subjected to full DFT optimization. The central structures obtained from DFT calculations are found to be similar to their corresponding X-ray structures for systems wherever comparison is possible (Table 4). DFT optimized structure of **2**, for which the X-ray structure is not available, is provided in Figure 10 and optimized coordinates are provided in the Supporting Information. It shows dinuclear metallamacrocycles involving two Ir(*ppy*)$_2$ units spanned by two linkers analogous to compounds **1** and **3**. In general, longer Ir···Ir distances were observed for DFT optimized structures compared to their X-ray counterparts although for **5** the two bond distances are nearly similar (Table 4).

Table 4. Ir···Ir Distances (Å) Obtained from X-ray Studies and DFT Optimization for Compounds 1−5

	compound				
	1	**2**	**3**	**4**	**5**
X-ray	9.878(1)		10.007(1)	5.124(1)	6.996(1)
DFT	10.117	12.636	10.360	5.706	6.985

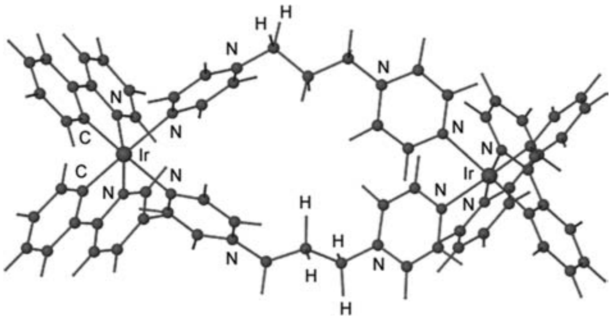

Figure 10. DFT optimized structure of **2**.

To gain insight into the electrochemical and photophysical behavior of these compounds, we examined their frontier orbitals carefully. The contour surfaces of the highest occupied molecular orbitals (HOMOs) and lowest unoccupied molecular orbitals (LUMOs) are provided in Figure 11. For all the cases, the HOMOs are primarily based on the ppy ligand with 26−36% contribution from one of the Ir dπ orbitals. The percentages of atomic contributions for Ir and spacers are collected in Table 5. The LUMOs are mainly centered on the linker ligand(s). However, some significant observations are made. For *bpa* and *bpe* linkers in compounds **1** and **2**, the contributions from the methylene (−CH$_2$−) carbons are practically zero (Table 5). On the contrary, the corresponding values for the carbon atoms of each of the −CH=CH− spacers are more than 6% indicating electron delocalization of the bridging *bpe* ligands in **3**. Dramatic increase in the contributions of the spacer atoms was observed for the *abp* bridge in compound **4**. Higher values were noted for the carbons (18.34, 18.28) than nitrogens (6.63, 6.79) in the −CH=N−N=CH− spacer. The atomic contributions calculated for the *bpfd* linker in **5** reveal that, as expected, the conjugation is restricted on the pyridyl-imine fragments truncated by the −CH$_2$−CH$_2$− spacers. The contributions from the methylene carbons are insignificant whereas the corresponding values for the carbons and nitrogens are 10−13%. This indicates delocalization only on the imine parts of the linker in **5** unlike compound **4** in which delocalization is noted throughout the bridge.

■ SUMMARY

Herein, we report three metallamacrocycles of general formula [{Ir(*ppy*)$_2$}$_2$(μ-BL)$_2$](OTf)$_2$ (**1**−**3**) and two open-frame dimers [{Ir(*ppy*)$_2$}$_2$(μ-BL)](OTf)$_2$ (**4**, **5**) containing cyclometalated "Ir(ppy)$_2$" units and different bis-pyridyl bridging ligands. The spacers linking two pyridyl groups in the bridging ligand (BL) dictate the structures and properties of the resulting compounds. Cyclic voltammetry experiments reveal weakly interacting "Ir(ppy)$_2$" units bridged by ethylene based *bpe* ligand in **3** whereas the metal centers are electronically isolated in **1** and **2** in which the bridging ligands are based on ethane and propane linkers. The dimer **4** exhibits two accessible reversible reductions in the cyclic voltammetric experiment indicating the stability of the one-electron reduced species located on diimine based bridge *abp*. The "Ir(ppy)$_2$" units in compound **5** are noninteracting as the electronic conduit is truncated by the ethane spacer in the *bpfd* bridge. The dinuclear compounds **1**−**5** show ligand-centered (LC) and mixed metal-to-ligand/ligand-to-ligand charge transfer (MLCT/LLCT) transitions. For the conjugated bridge *bpe* in compound **3** and *abp* in compound **4**, the lowest-energy charge transfer absorptions are red-shifted with enhanced extinction coefficients. In accordance with their similar electronic structures, compounds **1** and **2** exhibit nearly identical emissions composed of two bands and a shoulder covering the region about 450−600 nm. Compounds **3**−**5** show broad and unstructured emission, presumably from mixed ^{3}MLCT/^{3}LLCT emissive states. Compound **5** exhibits lower-energy emission and excitation bands in the solid state or frozen solutions from those in fluid acetonitrile solution, which was explained as a *syn-*/*anti-* conformational isomerism. DFT computations reveal that the Kohn−Sham HOMOs are primarily localized on the "Ir(ppy)$_2$" core with significant contributions from the metal. The Kohn−Sham LUMOs are predominantly located on the bridging ligand with different degrees of delocalization among their atoms, depending on the nature of the spacers. This is apparent from the computed atomic percentages (Mulliken analysis) constituting the spacers. The π-conjugated bridges *bpe* and *abp* in compounds **3** and **4** respectively, allow electronic communication between the metal centers and stabilize the LUMOs affording stability to the corresponding reduced species. Further, these bridges are responsible for the red-shifting of the CT absorption bands with enhanced intensities.

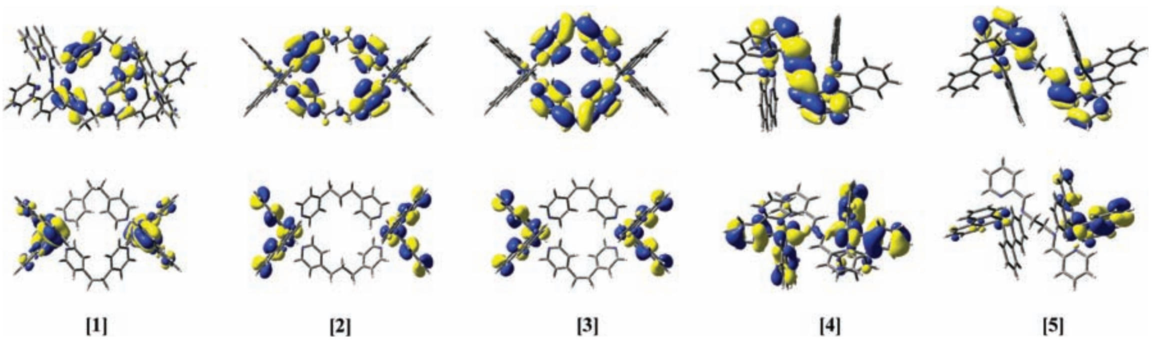

Figure 11. Contour surfaces of HOMOs (below) and LUMOs (top) computed for the DFT optimized structures of **1**−**5**.

Table 5. Atomic Percentages for the Ir and the Constituting Atoms of the Spacers

	HOMO	LUMO	
compound	Ir	spacer atoms	atomic percentages[a]
[**1**]	33	−C−C−	0.21, 0.22 (0.22, 0.21)
[**2**]	34	−C−C−C−	0.23, 0.42, 0.24 (0.32, 0.58, 0.28)
[**3**]	36	−C=C−	6.18, 6.15 (6.54, 6.57)
[**4**]	27	−C=N−N=C−	18.34, 6.63, 6.79, 18.28
[**5**]	26	-C=N−C−C−N=C−	12.60, 11.04, 0.97, 1.00, 10.50, 12.02

[a] The values in parentheses are for the second bridging ligand.

■ EXPERIMENTAL SECTION

Materials and Methods. All manipulations were carried out under an inert atmosphere with the use of standard Schlenk-line techniques. Glassware were dried prior to use. Solvents were dried by conventional methods, distilled over nitrogen, and deoxygenated prior to use. $IrCl_3{\cdot}3H_2O$ was purchased from Arora Matthey, India. Triflic acid, silver carbonate, 2-phenyl pyridine, 1,2-di(pyridin-4-yl)ethane, 1,2-di(pyridin-4-yl)propane, *trans*-1,2-di-(4-pyridyl)-ethylene, pyrazine were purchased from Aldrich and used as received. *N*,*N*′-bis-pyridin-2-ylmethylene-hydrazine[13] and *N*,*N*′-bis-pyridin-2-ylmethylene-ethane-1,2-diamine[14] were synthesized according to the literature procedure. Elemental analyses were carried out by using a Thermo quest CE instrument model EA/110 CHNS-O elemental analyzer. Infrared spectra were recorded in the range 4000−400 cm^{-1} on a Vertex 70 Bruker Spectrophotometer on KBR pellets. ^1H NMR spectra were obtained on a JEOL-JNM LAMDA 400 model and JEOL-DELTA2 500 model spectrometer. ^1H NMR chemical shifts were referenced to the residual hydrogen signal of the deuterated solvents. ESI-MS analyses were performed on a Waters Micromass Quattro Micro triple quadrupole mass spectrometer. UV−visible spectra were recorded using a Perkin-Elmer Lambda-20 UV/vis absorption spectrophotometer. Emission spectra were recorded using a Fluorolog FL3-21(Horiba Jobin Yvon) spectrofluorometer equipped with a xenon flash lamp and also using a PTI QuantaMaster Model QM-4 scanning spectrofluorometer equipped with a 75-W xenon lamp, emission and excitation monochromators, excitation correction unit, and a PMT detector for both visible and near-IR regions. The excitation and emission spectra have been corrected for the wavelength-dependent lamp intensity and detector response, respectively; corrected versus uncorrected spectra for the fluid and frozen solutions are shown in the Supporting Information (Figures S5 and S6) whereas only corrected spectra are shown in the main manuscript. Emission quantum yields were determined by comparison with the emission of a solution of quinine sulfate ($\Phi = 0.545$) in 1N of H_2SO_4, employed as a standard.[15] The excitation wavelength used was 350 nm. The quantum yields were then calculated using the expression, $\Phi_S = \Phi_R(A_S/A_R)(n_S{}^2/n_R{}^2)$. Here, the subscripts S and R denote sample and reference respectively, Φ is the fluorescence quantum yield, *A* is the integrated area under the corrected fluorescence spectra, *n* is the refractive index of the solvent.

Cyclic voltammetric studies were performed on a BAS Epsilon electrochemical workstation in acetonitrile with 0.1 M tetra-*n*-butylammonium hexafluorophosphate ($TBAPF_6$) as the supporting electrolyte. The working electrode was a BAS Pt disk electrode, the reference electrode was Ag/AgCl, and the auxiliary electrode was a Pt wire. The ferrocene/ferrocenium couple occurs at $E_{1/2} = +0.51$ (70) V versus Ag/AgCl under the same experimental conditions. The potentials are reported in volts (V); the ΔE ($E_{p,a} - E_{p,c}$) values are in millivolts (mV) at a scan rate 100 mV s^{-1}.

X-ray Data Collection and Refinement. Single-crystal X-ray studies were performed on a CCD Bruker SMART APEX diffractometer equipped with an Oxford Instruments low-temperature attachment. All the data were collected at 100(2) K using graphite-monochromated Mo−Kα radiation ($\lambda\alpha$ = 0.71073 Å). The frames were indexed, integrated, and scaled using the SMART and SAINT software packages,[16] and the data were corrected for absorption using the SADABS program.[17] The structures were solved and refined with the SHELX suite of programs.[18] All hydrogen atoms were included in the final stages of the refinement and were refined with a typical riding model. Structure solution and refinement details for compounds **1**, **3**, **4**, and **5** are provided in the Supporting Information. All non-hydrogen atoms were refined with anisotropic thermal parameters. The "SQUEEZE" option in PLATON program[19] was used to remove a disordered solvent molecule from the overall intensity data of compound **1**, **3**, and **5**. Pertinent crystallographic data are summarized in Table 6. ORTEP-32[20] was used to produce the diagrams. CCDC−816040 (**1**), 816041 (**3**), 816042 (**4**), and 816043 (**5**) contain the supplementary crystallographic data for this paper. These data can be obtained free of charge from the Cambridge Crystallographic Data Centre via www.ccdc.cam.ac.uk/data_request/cif.

Theoretical Study. Calculations were performed using density functional theory (DFT) with Becke's three parameter hybrid exchange functional[21] and the Lee−Yang−Parr correlation functional (B3LYP).[22] Geometry optimized structures were characterized fully via analytical frequency calculations as minima on the potential energy surface. The double-ζ basis set of Hay and Wadt (LanL2DZ) with a small core (1s2s2p3s3p3d4s4p4d) effective core potential (ECP)[23] was used for the Ir. The ligand atoms H, C, N, and O atoms were described using the 6-31G(d,p) basis sets. All calculations were performed with the Gaussian 03 (G03)[24] suite of programs. Gaussview 3.0 was used for generating the orbital plots.

Synthesis. The syntheses of **1**−**5** were carried out by using a similar procedure. As a representative example the synthesis of **1** is given in detail. The details for specific reactions are given below.

*[{Ir(ppy)$_2$}$_2$(μ-bpa)$_2$](OTf)$_2$ (**1**).* A mixture containing $[(ppy)_2Ir(\mu\text{-}Cl)]_2$ (100 mg, 0.09 mmol) and AgOTf (50 mg, 0.20 mmol) in 20 mL of acetone was refluxed under N_2 for 2 h. The yellow slurry was allowed to cool, and AgCl was removed by filtration. The filtrate was evaporated to dryness under reduced pressure to get yellow oil. The oily mass was redissolved in 20 mL of 1,2-dichloroethane-(DCE) followed by the addition of *bpa* (37 mg, 0.20 mmol)). This solution was heated under reflux for 12 h under a N_2 atmosphere.

Table 6. Crystallographic Data and Pertinent Refinement Parameters for Compounds **1**, **3**, **4**, and **5**

	$1\cdot4CH_3CN$	$3\cdot3.5H_2O$	$4\cdot CH_2Cl_2$	5
empirical formula	$C_{78}H_{68}F_6Ir_2N_{12}O_6S_2$	$C_{70}H_{52}F_6Ir_2N_8O_{9.5}S_2$	$C_{59}H_{44}Cl_2F_6Ir_2N_8O_6S_2$	$C_{60}H_{46}F_6Ir_2N_8O_6S_2$
formula weight	1831.96	1719.78	1594.44	1537.57
crystal system	monoclinic	monoclinic	monoclinic	monoclinic
space group	$C2/c$	$P2_1/c$	$P2_1/c$	$P2_1/c$
a, Å	21.1749(17)	19.2549(15)	17.4100(16)	14.866(4)
b, Å	19.4858(17)	42.139(3)	14.6706(14)	13.167(3)
c, Å	19.0358(17)	10.8346(9)	22.612(2)	17.161(4)
α, deg	90.00	90.00	90.00	90.00
β, deg	97.544(2)	103.904(2)	91.850(2)	108.725(4)
γ, deg	90.00	90.00	90.00	90.00
V, Å^3	7786.4(12)	8533.4(11)	5772.4(9)	3181.3(13)
Z	4	4	4	2
ρ_{calcd}, g cm^{-3}	1.563	1.339	1.835	1.605
μ, mm^{-1}	3.542	3.229	4.850	4.315
$F(000)$	3632	3376	3104	1500
reflections				
collected	26641	43334	38867	24217
independent	6623	14510	9811	6504
observed $[I > 2\sigma(I)]$	5067	7821	8350	5394
no. of variables	480	848	766	379
goodness-of-fit	0.964	1.032	1.052	1.041
final R indices $[I > 2\sigma(I)]^a$				
R1	0.0366	0.1067	0.0408	0.0358
wR2	0.0800	0.2786	0.1009	0.0938
R indices (all data)^a				
R1	0.0524	0.1823	0.0497	0.0435
wR2	0.0864	0.3229	0.1063	0.0985

[a] $R_1 = \sum||F_o| - |F_c||/\sum|F_o|$ with $F_o^2 > 2\sigma(F_o^2)$. $wR_2 = [\sum w(F_o^2 - F_c^2)^2/\sum|F_o^2|^2]^{1/2}$.

Subsequently, the volume of the bright yellow colored solution was reduced to ~2 mL and diethyl ether was added to induce precipitation and solid precipitate was filtered, washed with diethyl ether (5 mL, 3 times), and dried in vacuum. This compound was identified as **1**. Crystals suitable for X-ray data collection were obtained by layering diethyl ether onto the saturated acetonitrile solution of **1**. Yield: 127 mg (81.7%). Anal. Calc. for $C_{70}H_{56}F_6Ir_2N_8O_6S_2$: C, 50.41; H, 3.38; N, 6.71%. Found: C, 50.04; H, 3.70; N, 6.43%. ^{1}H NMR ($CDCl_3$, 500 MHz, δ): 8.77 (d, 4H), 8.43 (d, 8H), 7.70 (t, 4H), 7.62 (d, 4H), 7.45 (t, 4H), 7.32 (q, 4H), 6.88 (d, 8H), 6.77 (m, 8H), 6.23 (m, 4H), 2.89 (d, 4H), 2.49 (d, 4H). IR (KBr, ν cm^{-1}): 3463(br), 3045(w), 2927(w), 2853(w), 1611 (m), 1480 (s), 1423 (m), 1264 (vs), 1159 (m), 1030 (vs), 758 (m), 638 (m). ESI-MS: m/z 1520 for $[\{M\}^{2+}+\mathrm{OT\bar{f}}]^+$.

[{Ir(ppy)$_2$}$_2$(μ-bpp)$_2$](OTf)$_2$ **(2)**. The reaction of $[(ppy)_2Ir(\mu\text{-}Cl)]_2$ (100 mg, 0.09 mmol), AgOTf (50 mg, 0.20 mmol), and bpp (40 mg, 0.20 mmol) was carried out following a procedure similar to that described for the synthesis of **1**. Yield: 123 mg (77.8%). Anal. Calc. for $C_{72}H_{60}F_6Ir_2N_8O_6S_2$: C, 50.99; H, 3.56; N; 6.60%. Found: C, 50.72; H, 3.27; N, 6.76%. ^{1}H NMR ($CDCl_3$, 500 MHz, δ): 8.7(d, 4H), 8.27 (d, 8H), 7.79−7.62 (m, 8H), 7.43 (t, 4H), 7.32−7.19 (m, 12H), 6.85 (d, 8H), 6.31 (m, 4H), 2.60 (m, 8H), 1.99 (m, 4H). IR (KBr, ν cm^{-1}): 3483(br), 3045(w), 2928(w), 2850(w), 1611(m), 1480(m), 1423(m), 1266(vs), 1158(m), 1030(vs), 759(m), 637(m). ESI-MS: m/z 1547 for $[\{M\}^{2+}+\mathrm{OT\bar{f}}]^+$.

[{Ir(ppy)$_2$}$_2$(μ-bpe)$_2$](OTf)$_2$ **(3)**. The reaction of $[(ppy)_2Ir(\mu\text{-}Cl)]_2$ (100 mg, 0.09 mmol), AgOTf (50 mg, 0.20 mmol), and *bpe* (37 mg, 0.20 mmol) was carried out following a procedure similar to that described for the synthesis of **1**. The volume of the orange colored solution was reduced to ~5 mL and kept it for crystallization. Yield: 75 mg (48%). Anal. Calc. for $C_{70}H_{52}F_6Ir_2N_8O_6S_2$: C, 50.53; H, 3.15; N, 6.73%. Found: C, 50.71; H, 3.13; N, 6.67%. ^{1}H NMR (CD_3CN, 500 MHz, δ): 8.6 (d, 4H), 8.49(d, 8H), 7.89(t, 4H), 7.7(d, 4H), 7.58−7.33 (m, 16H), 7.28 (d, 2H), 7.25(d, 2H), 6.88 (d, 8H), 6.26(d, 4H). IR (KBr, ν cm^{-1}): 3451(br), 3046(w), 1609(s), 1479(m), 1422(m), 1264(vs), 1161(m), 1030(s), 760(m), 638(m). ESI-MS: m/z 1515 for $[\{M\}^{2+}+\mathrm{OT\bar{f}}]^+$.

[{Ir(ppy)$_2$}$_2$(μ-abp)](OTf)$_2$ **(4)**. The reaction of $[(ppy)_2Ir(\mu\text{-}Cl)]_2$ (100 mg, 0.09 mmol), AgOTf (50 mg, 0.20 mmol), and *abp* (23 mg, 0.10 mmol) was carried out following a procedure similar to that described for the synthesis of **1**. Analytically pure dark green compound was obtained by crystallization from dichloromethane/hexane mixture. Yield: 112 mg (80%). Anal. Calc. for $C_{58}H_{42}F_6Ir_2N_8O_6S_2$: C, 46.14; H, 2.80; N, 7.42%. Found: C, 46.06; H, 2.51; N, 7.21%. ^{1}H NMR (CD_3CN,500 MHz, δ): 9.48(s, 1H); 9.12(s, 1H), 8.43(d, 1H), 8.17 (d, 1H), 8.00−7.80 (m, 6H), 7.72−7.54 (m, 3H), 7.43−7.38 (m, 4H), 7.21−7.13 (m, 4H), 7.01−6.69 (m, 16H), 6.42 (d, 1H), 6.15 (d, 1H), 5.73 (d, 1H), 5.52 (d, 1H), 5.31 (d, 1H). IR (KBr, ν cm^{-1}): 3456(br), 3052(w), 2920, 1627, 1608(s), 1582, 1479(m), 1421(m), 1261(vs), 1158(m), 1029(s), 757(m), 636(m). ESI-MS: m/z 1361 for $[\{M\}^{2+}+\mathrm{OT\bar{f}}]^+$; m/z (z = 2) 605 for $[M]^{2+}$.

[{Ir(ppy)$_2$}$_2$(μ-bpfd)](OTf)$_2$ **(5)**. The reaction of $[(ppy)_2Ir(\mu\text{-}Cl)]_2$ (100 mg, 0.09 mmol), AgOTf (50 mg, 0.20 mmol), and *bped* (25 mg, 0.10 mmol) was carried out following a procedure similar to that described for the synthesis of **1**. Analytically pure compound was obtained by crystallization from chloroform/diethyl ether mixture. Yield: 102 mg (71%). Anal. Calc. for $C_{60}H_{46}F_6Ir_2N_8O_6S_2$: C, 46.86; H, 3.01; N; 7.28%. Found: C, 46.52; H, 3.11; N, 7.38%. ^{1}H NMR (CD_3CN, 500 MHz, δ): 8.17(d, 1H), 8.07−7.69 (m, 20H), 7.57 (d, 1H), 7.47 (t, 2H), 7.34 (t, 2H), 7.17−7.04 (m, 6H), 6.99−6.82 (m, 6H), 6.29 (d, 1H), 6.09 (d, 1H), 5.99 (dd, 2H), 3.48 (m, 2H), 3.26 (m, 2H). IR (KBr, ν cm^{-1}): 3483(br), 3042(w), 2923, 1629, 1606(s), 1478(m), 1438(m), 1263(vs), 1154(m), 1030(vs), 758(m), 636(m). ESI-MS: m/z 1389 for $[\{M\}^{2+}+\mathrm{OT\bar{f}}]^+$; m/z (z = 2) 619 for $[M]^{2+}$.

■ ASSOCIATED CONTENT

Ⓢ Supporting Information

Further crystallographic (CIF format) and ESI-MS, electrochemical, photophysical, and computational data (PDF format).

This material is available free of charge via the Internet at http://pubs.acs.org.

Dedication

$^\perp$Dedicated to the memory of Oussama Elbjeirami, a co-author of this paper, who passed away prematurely.

AUTHOR INFORMATION

Corresponding Author

*E-mail: vc@iitk.ac.in (V.C.), jbera@iitk.ac.in (J.K.B.), omary@unt.edu (M.A.O.).

ACKNOWLEDGMENTS

IITK authors are grateful to the Defense Research Development Organization, New Delhi, for financial support. V.C. is grateful to the Department of Science and Technology for a National J. C. Bose Fellowship. T.H. is grateful to the University Grants Commission, New Delhi, for a Senior Research Fellowship. M.A.O. acknowledges partial support of his contribution by the National Science Foundation (CHE-0911690; DMR-0805089; CMMI-0963509; CHE-0840518) and the Robert A. Welch Foundation (Grant B-1542).

REFERENCES

(1) (a) Aguirre-Etcheverry, P.; O'Hare, D. *Chem. Rev.* **2010**, *110*, 4839,and references therein. (b) Liu, W.; Lee, V.; Park, M.; John, R. P.; Moon, D.; Zou, Y.; Liu, X.; Ri, H.-C.; Kim, G. H.; Lah, M. S. *Inorg. Chem.* **2008**, *47*, 8807. (c) King, P.; Stamatatos, T. C.; Abboud, K. A.; Christou, G. *Angew. Chem., Int. Ed.* **2006**, *45*, 7379. (d) Wang, P.; Moorefield, C. N.; Newkome, G. R. *Angew. Chem., Int. Ed.* **2005**, *44*, 1679. (e) Yuan, Q.-H.; Wan, L.-J.; Jude, H.; Stang, P. J. *J. Am. Chem. Soc.* **2005**, *127*, 16279. (f) Sautter, A.; Kaletas, B. K.; Schmid, D. G.; Dobrawa, R.; Zimine, M.; Jung, G.; van Stokkum, I. H. M.; De Cola, L.; Williams, R. M.; Würthner, F. *J. Am. Chem. Soc.* **2005**, *127*, 6719. (g) Patel, U.; Singh, H. B.; Wolmershäuser, G. *Angew. Chem., Int. Ed.* **2005**, *44*, 1715. (h) Tasiopoulos, A. J.; Vinslava, A.; Wernsdorfer, W.; Abboud, K. A.; Christou, G. *Angew. Chem., Int. Ed.* **2004**, *43*, 2117. (i) Dendrinou-Samara, C.; Zaleski, C. M.; Evagorou, A.; Kampf, J. W.; Pecoraro, V. L.; Kessissoglou, D. P. *Chem. Commun.* **2003**, 2668. (j) Wang, X.; Vittal, J. J. *Inorg. Chem.* **2003**, *42*, 5135. (k) Bodwin, J. J.; Cutland, A. D.; Malkani, R. G.; Pecoraro, V. L. *Coord. Chem. Rev.* **2001**, *216–217*, 489.

(2) (a) Das, A. K.; Sarkar, B.; Fiedler, J.; Zális, S.; Hartenbach, I.; Strobel, S.; Lahiri, G. K.; Kaim, W. *J. Am. Chem. Soc.* **2009**, *131*, 8895. (b) Brocker, E. R.; Anderson, S. E.; Northrop, B. H.; Stang, P. J.; Bowers, M. T. *J. Am. Chem. Soc.* **2010**, *132*, 13486. (c) Ghosh, S.; Chakrabarty, R.; Mukherjee, P. S. *Inorg. Chem.* **2009**, *48*, 549. (d) Blanco, V.; Gutiérrez, A.; Platas-Iglesias, C.; Peinador, C.; Quintela, J. M. *J. Org. Chem.* **2009**, *74*, 6577. (e) Fujita, M.; Yazaki, J.; Ogura, K. *J. Am. Chem. Soc.* **1990**, *112*, 5645. (f) Caskey, D. C.; Yamamoto, T.; Addicott, C.; Shoemaker, R. K.; Vacek, J.; Hawkridge, A. M.; Muddiman, D. C.; Kottas, G. S.; Michl, J.; Stang, P. J. *J. Am. Chem. Soc.* **2008**, *130*, 7620. (g) Weilandt, T.; Troff, R. W.; Saxell, H.; Rissanen, K.; Schalley, C. A. *Inorg. Chem.* **2008**, *47*, 7588.

(3) (a) Shin, C. H.; Huh, J. O.; Baek, S. J.; Kim, S. K.; Lee, M. H.; Do, Y. *Eur. J. Inorg. Chem.* **2010**, 3642. (b) Whittle, V. L.; Williams, J. A. G. *Inorg. Chem.* **2008**, *47*, 6596. (c) Han, Y.-F.; Lin, Y.-J.; Jia, W.-G. ; Weng, L.-H.; Jin, G.-X. *Organometallics* **2007**, *26*, 5848. (d) Lafolet, F.; Welter, S.; Popović, Z.; De Cola, L. *J. Mater. Chem.* **2005**, *15*, 2820. (e) Cavazzini, M.; Pastorelli, P.; Quici, S.; Loiseau, F.; Campagna, S. *Chem. Commun.* **2005**, 5266. (f) Tsuboyama, A.; Takiguchi, T.; Okada, S.; Osawa, M.; Hoshino, M.; Ueno, K. *Dalton Trans.* **2004**, 1115. (g) Plummer, E. A.; Hofstraat, J. W.; De Cola, L. *Dalton Trans.* **2003**, 2080. (h) Neve, F.; Crispini, A.; Serroni, S.; Loiseau, F.; Campagna, S. *Inorg. Chem.* **2001**, *40*, 1093. (i) Dixon, I. M.; Sauvage, J.-P.; Flamigni, L.; Susana, E.; Barigelletti, F. *Chem. Soc. Rev.* **2000**, *29*, 385.

(4) (a) Flamigni, L.; Barbieri, A.; Sabatini, C.; Ventura, B.; Barigelletti, F. *Top. Curr. Chem.* **2007**, *281*, 143. (b) You, Y.; Park, S. Y. *Dalton Trans.* **2009**, 1267. (c) Wong, W.-Y.; Ho, C.-L. *Coord. Chem. Rev.* **2009**, *253*, 1709. (d) Lowry, M. S.; Bernhard, S. *Chem.—Eur. J.* **2006**, *12*, 7970. (e) Ulbricht, C.; Beyer, B.; Friebe, C.; Winter, A.; Schubert, U. S. *Adv. Mater.* **2009**, *21*, 4418.

(5) Nonoyama, M. *Bull. Chem. Soc. Jpn.* **1974**, *47*, 767.

(6) Johnston, D. H.; Shriver, D. F. *Inorg. Chem.* **1993**, *32*, 1045.

(7) Auffrant, A.; Barbieri, A.; Barigelletti, F.; Lacour, J.; Mobian, P.; Collin, J.-P.; Sauvage, J.-P.; Ventura, B. *Inorg. Chem.* **2007**, *46*, 6911.

(8) (a) Nazeeruddin, M. K.; Wegh, R. T.; Zhou, Z.; Klein, C.; Wang, Q.; Angelis, F. D.; Fantacci, S.; Grätzel, M. *Inorg. Chem.* **2006**, *45*, 9245. (b) Neve, F.; Deda, M. L.; Crespini, A.; Bellusci, A.; Puntoriero, F.; Campagna, S. *Organometallics* **2004**, *23*, 5856. (c) Lepeltier, M.; Lee, T. K.-M.; Lo, K. K.-W.; Toupet, L.; Bozec, H. L.; Guerchais, V. *Eur. J. Inorg. Chem.* **2005**, 110. (d) Goldsmith, J. I.; Hudson, W. R.; Lowry, M. S.; Anderson, T. H.; Bernhard, S. *J. Am. Chem. Soc.* **2005**, *127*, 7502. (e) Neve, F.; Deda, M. L.; Puntoriero, F.; Campagna, S. *Inorg. Chim. Acta* **2006**, *359*, 1666. (f) Bolink, H. J.; Cappelli, L.; Coronado, E.; Grätzel, M.; Ortí, E.; Costa, R. D.; Viruela, P. M.; Nazeeruddin, M. K. *J. Am. Chem. Soc.* **2006**, *128*, 14786. (g) Angelis, F. D.; Fantacci, S.; Evans, N.; Klein, C.; Zakeeruddin, S. M.; Moser, J.-E.; Kalyanasundaram, K.; Bolink, H. J.; Grätzel, M.; Nazeeruddin, M. K. *Inorg. Chem.* **2007**, *46*, 5989. (h) King, K. A.; Watts, R. J. *J. Am. Chem. Soc.* **1987**, *109*, 1589. (i) Costa, R. D.; Orti, E.; Bolink, H. J.; Graber, S.; Housecroft, C. E.; Constable, E. C. *J. Am. Chem. Soc.* **2010**, *132*, 5978.

(9) (a) Zhou, X.-H.; Wu, T.; Li, D. *Inorg. Chim. Acta* **2006**, *359*, 1442. (b) Singh, A.; Chandra, M.; Sahay, A. N.; Pandey, D. S.; Pandey, K. K.; Mobin, S. M.; Puerta, M. C.; Valerga, P. *J. Organomet. Chem.* **2004**, *689*, 182.

(10) (a) Calogero, G.; Giuffrida, G.; Serroni, S.; Ricevuto, V.; Campagna, S. *Inorg. Chem.* **1995**, *34*, 541. (b) Lowry, M. S.; Goldsmith, J. I.; Slinker, J. D.; Rohl, R.; Pascal, R. A. Jr.; Malliaras, G. G.; Bernhard, S. *Chem. Mater.* **2005**, *17*, 5712. (c) Dragonetti, C.; Falciola, L.; Mussini, P.; Righetto, S.; Roberto, D.; Ugo, R.; Valore, A.; De Angelis, F.; Fantacci, S.; Sgamellotti, A.; Ramon, M.; Muccini, M. *Inorg. Chem.* **2007**, *46*, 8533.

(11) Chin, C. S.; Eum, M.-S. ; Kim, S. Y.; Kim, C.; Kang, S. K. *Eur. J. Inorg. Chem.* **2007**, 372.

(12) Lowry, M. S.; Hudson, W. R.; Pascal, R. A.; Bernhard, S. *J. Am. Chem. Soc.* **2004**, *126*, 14129.

(13) Kennedy, A. R.; Brown, K. G.; Graham, D.; Kirkhouse, J. B.; Kittner, M.; Major, C.; McHugh, C. J.; Murdoch, P.; Smith, W. E. *New J. Chem.* **2005**, *29*, 826.

(14) (a) Karmakar, T. K.; Chandra, S. K.; Ribas, J.; Mostafa, G.; Lu, T. -H.; Ghosh, B. K. *Chem. Commun.* **2002**, 2364. (b) Baar, C. R.; Jennings, M. C.; Vittal, J. J.; Puddephatt, R. J. *Organometallics* **2000**, *19*, 4150.

(15) Berlman, I. B. *Handbook of Fluorescence Spectra of Aromatic Molecules*; Academic Press: New York, 1965.

(16) *SAINT+ Software for CCD Difractometers*; Bruker AXS: Madison, WI, 2000.

(17) Sheldrick, G. M. *SADABS Program for Correction of Area Detector Data*; University of Göttingen: Göttingen, Germany, 1999.

(18) (a) *SHELXTL*, Package v. 6.10; Bruker AXS: Madison, WI, 2000. (b) Sheldrick, G. M. *SHELXS-86 and SHELXL-97*; University of Göttingen: Göttingen, Germany, 1997.

(19) Spek, A. L. *PLATON*; University of Utrecht: Utrecht, The Netherlands, 2001.

(20) Farrugia, L. J. *J. Appl. Crystallogr.* **1997**, *30*, 565.

(21) Parr, R. G.; Yang, W. *Density-Functional Theory of Atoms and Molecules*; Oxford University Press: Oxford, U.K., 1989.

(22) (a) Becke, A. D. *J. Chem. Phys.* **1993**, *98*, 5648. (b) Lee, C.; Yang, W.; Parr, R. G. *Phys. Rev. B* **1998**, *37*, 785.

(23) (a) Hay, P. J.; Wadt, W. R. *J. Chem. Phys.* **1985**, *82*, 270. (b) Wadt, W. R.; Hay, P. J. *J. Chem. Phys.* **1985**, *82*, 284. (c) Hay, P. J.; Wadt, W. R. *J. Chem. Phys.* **1985**, *82*, 299.

(24) Frisch, M. J.; Trucks, G. W.; Schlegel, H. B.; Scuseria, G. E.; Robb, M. A.; Cheeseman,Jr. J. R.; Montgomery, J. A.; Vreven, T.; Kudin, K. N.; Burant, J. C.; Millam, J. M.; Iyengar, S. S.; Tomasi, J.; Barone, V.; Mennucci, B.; Cossi, M.; Scalmani, G.; Rega, N.; Petersson, G. A.; Nakatsuji, H.; Hada, M.; Ehara, M.; Toyota, K.; Fukuda, R.; Hasegawa, J.; Ishida, M.; Nakajima, T.; Honda, Y.; Kitao, O.; Nakai, H.; Klene, M.; Li, X.; Knox, J. E.; Hratchian, H. P.; Cross, J. B.; Adamo, C.; Jaramillo, J.; Gomperts, R.; Stratmann, R. E.; Yazyev, O.; Austin, A. J.; Cammi, R.; Pomelli, C.; Ochterski, J. W.; Ayala, P. Y.; Morokuma, K.; Voth, G. A.; Salvador, P.; Dannenberg, J. J.; Zakrzewski, V. G.; Dapprich, S.; Daniels, A. D.; Strain, M. C.; Farkas, O.; Malick, D. K.; Rabuck, A. D.; Raghavachari, K.; Foresman, J. B.; Ortiz, J. V.; Cui, Q.; Baboul, A. G.; Clifford, S.; Cioslowski, J.; Stefanov, B. B.; Liu, G.; Liashenko, A.; Piskorz, P.; Komaromi, I.; Martin, R. L.; Fox, D. J.; Keith, T.; Al-Laham, M. A.; Peng, C. Y.; Nanayakkara, A.; Challacombe, M.; Gill, P. M. W.; Johnson, B.; Chen, W.; Wong, M. W.; Gonzalez, C.; Pople, J. A. *Gaussian 03*; Gaussian, Inc.: Pittsburgh, PA, 2003.